Special Section: Model-Data Fusion in the Vadose Zone

Francesco Ciocca*
Ivan Lunati
Nick Van de Giesen
Marc B. Parlange

An Actively Heated Fiber Optics method is tested to estimate soil moisture profiles along 30 meters of fiber optic cable buried in a large coil in a lysimeter variably saturated with depth. A comparison with independent soil moisture measurements shows an excellent matching in wet soil, while a significant underestimation occurs in dry conditions.

F. Ciocca, School of Architecture, Civil and Environmental Engineering, EPF, Lausanne, Switzerland; I. Lunati, Institute of Geophysics, Univ. of Lausanne, Switzerland; N. Van de Giesen, Faculty of Civil Engineering and Geosciences, TU Delft, Netherlands; M.B. Parlange, School of Architecture, Civil and Environmental Engineering, EPF, Lausanne, Switzerland. *Corresponding author (francesco.ciocca@epfl.ch).

Vadose Zone J.
doi:10.2136/vzj2011.0199
Received 20 Dec. 2011.
Open Access Article

Heated Optical Fiber for Distributed Soil-Moisture Measurements: A Lysimeter Experiment

An Actively Heated Fiber Optics (AHFO) method to estimate soil moisture is tested and the analysis technique improved on. The measurements were performed in a lysimeter uniformly packed with loam soil with variable water content profiles. In the first meter of the soil profile, 30 m of fiber optic cable were installed in a 12 loops coil. The metal sheath armoring the fiber cable was used as an electrical resistance heater to generate a heat pulse, and the soil response was monitored with a Distributed Temperature Sensing (DTS) system. We study the cooling following three continuous heat pulses of 120 s at 36 W m^{-1} by means of long-time approximation of radial heat conduction. The soil volumetric water contents were then inferred from the estimated thermal conductivities through a specifically calibrated model relating thermal conductivity and volumetric water content. To use the pre-asymptotic data we employed a time correction that allowed the volumetric water content to be estimated with a precision of 0.01–0.035 (m^3 m^{-3}). A comparison of the AHFO measurements with soil-moisture measurements obtained with calibrated capacitance-based probes gave good agreement for wetter soils [discrepancy between the two methods was less than 0.04 (m^3 m^{-3})]. In the shallow drier soils, the AHFO method underestimated the volumetric water content due to the longer time required for the temperature increment to become asymptotic in less thermally conductive media [discrepancy between the two methods was larger than 0.1 (m^3 m^{-3})]. The present work suggests that future applications of the AHFO method should include longer heat pulses, that longer heating and cooling events are analyzed, and, temperature increments ideally be measured with higher frequency.

Abbreviations: AHFO, Active Heated Fiber Optics method; CB, capacitance-based; DTS, distributed temperature sensing; I_{AS}, Anti-Stokes intensity ; I_S, Stokes intensity; TDR, time domain reflectometry.

In recent years, optical fiber distributed temperature sensing (DTS) based on Raman scattering has been increasingly employed in environmental monitoring (e.g., Selker et al., 2006a; Selker et al., 2006b; Westhoff et al., 2007; Freifeld et al., 2008; Tyler et al., 2008, 2009; Vercauteren et al., 2011; Keller et al., 2011). DTS has proven accurate to measure temperature along the entire fiber optic cable (whose length can exceed 30,000 m), affording a spatial resolution of 1 m and temporal frequencies greater than one measurement per minute.

DTS has also been used to estimate distributed thermal properties from the response to the diurnal temperature cycle (Steele-Dunne et al., 2010). Despite the attractive simplicity of DTS, which only requires the burial of the cable, the application is limited to conditions where there is a sensitive response to the diurnal cycle (e.g., sunny days, top bare soil, etc.). To overcome these limitations, variants have been proposed in which DTS is used to monitor the soil response to active heating of the metal sheath that protects the optical fiber (Active Heated Fiber Optics method, AHFO). This method has been used to track groundwater water movement (e.g., Perzlmaier et al., 2004, 2006; Aufleger et al., 2005) and to measure soil moisture, where it has proven successful in distinguishing between dry, wet, and saturated soils (Weiss, 2003; Perzlmaier et al., 2004, 2006). This application of AHFO potentially offers an alternative to more established techniques to measure soil moisture such as capacitance-based (CB) probes (see, e.g., Nadler and Lapid, 1996; Mohamed et al., 1997; Seyfried and Murdock, 2001, 2004) or Time Domain Reflectometry (TDR) (see, e.g., Topp et al., 1980; Campbell, 1990; Topp et al., 2000; Robinson et al., 2003; Jones and Or, 2004; Seyfried and Murdock, 2004; Assouline et al., 2010). A review of the state-of-the-art of soil moisture measurement techniques was presented by Hopmans et al. (1999) and Robinson et al. (2008).

Weiss (2003) showed that it is possible to infer the water content from the soil-temperature response to active heating. The thermal properties of the soil were obtained through the

classical probe method, which is based on an asymptotic analysis of the thermal response (see, e.g., Carslaw and Jaeger, 1959; deVries and Peck, 1958), and the water content was inferred using a calibration equation. However, the method was unable to detect changes of soil moisture below 6%.

More recently, Sayde et al. (2010) proposed a different approach which requires, in addition to DTS, independent measurements of water content. They obtained an empirical calibration curve by fitting the temperature increase as a function of the measured water content and suggested that this procedure might lead to more accurate water-content estimates by avoiding the use and consequent inversion of thermal properties.

However, the calibration curve depends heavily on the soil type and on the experimental setup (e.g., pulse duration and specific characteristic of the fiber optic cable), and lacks a clear physical relationship between the coefficients and the physical parameters.

In this study, we test the AHFO technique using a large vertical coil installed within a lysimeter filled with loamy soil and we measure the spatial variability of the soil moisture. Similar to Weiss (2003), we apply the cylindrical probe method (see, e.g., Carslaw and Jaeger, 1959; deVries and Peck, 1958) to analyze the temperature evolution and estimate the thermal conductivity along the cable. To improve the estimate of the thermal properties, we introduce a time correction (Van der Held and Van Drunen, 1949; deVries, 1952; Shiozawa and Campbell, 1990; Bristow et al., 1994) that allows reducing the duration of the heat pulse and the consequent possible perturbation of the water content. The volumetric water content is obtained by inverting the thermal conductivity model of Lu et al. (2007), with parameters specifically calibrated for our soil. The results were compared with independent soil moisture measurements made with capacitance sensors installed at several depths in the lysimeter.

Theoretical Background

Raman Backscattering and DTS Measurements

When a pulsed laser beam propagates through a fiber optic cable, a portion of the photons are backscattered and collected by a photodetector that quantifies their intensity and the elapsed time between emission and detection. Any inhomogeneity of the optical fiber causes backscattering; in addition to the cable end and possible ruptures of the cable, impurities and density fluctuations contribute to the return signal measured by the photodetector. In all of these cases photons are usually backscattered at wavelength equal to wavelength of the incident laser beam (λ_o = 1064 nm in our case). This elastic scattering is referred to as Rayleigh (elastic) backscatter and involves the largest portion of the energy of the returning light.

In addition to the elastic backscattering, a less intense, inelastic backscattering occurs in the optical fiber, which is associated with the Raman effect and produces return signals of a different wavelength than the incident beam. The signal characterized by a wavelength $\lambda_S > \lambda_o$ is called the Stokes component, whereas the signal with wavelength $\lambda_A < \lambda_o$ is called the Anti-Stokes component. The ratio between the intensity of these two components (equally spaced from λ_o) depends on the temperature. While Stokes backscattering is generated by silica molecules that are in the vibrational ground state, Anti-Stokes backscattering requires the molecule to be in a vibrational excited state and, therefore, increases with the thermal excitation. The ratio between the intensities of Anti-Stokes (I_{AS}) and Stokes (I_S) components depends exponentially on the temperature, T [i.e., $I_{AS}/I_S \sim \exp(-\Delta E/k_B T)$, where ΔE is the energy shift from the Rayleigh peak and k_B the Boltzmann constant]. Therefore, the temperature can be inferred from the relative intensity of the Anti-Stokes to Stokes components.

A sufficient number of photons have to be collected to obtain a satisfactory signal-to-noise ratio and thus accurate temperature measurements. This determines the minimum time over which photons have to be collected and the maximum spatial resolution achievable by DTS. Usually, the lower limit to guarantee a good signal/noise ratio is on the order of 1 m (e.g., Weiss, 2003; Sayde et al., 2010), which is the distance over which the temperature is averaged in DTS measurements. We refer to Gratton and Meggitt (2000), Selker et al. (2006a, 2006b), and Tyler et al. (2009) for more details about the physical principle of DTS.

Estimation of Thermal Properties by the Probe Method

If an accurate technique to measure temperature is available, the thermal properties of the soil can be inferred from the temperature response to heating. In AHFO, the fiber optic cable is used both as a temperature sensor (exploiting the dependence of the Raman scattering on temperature) and as a heat source by generating an electric current in the metal sheath that protects the fiber.

The problem of a line heat source in a homogeneous medium is well known and has given origin to the probe method to measure the thermal conductivity of soil (see, e.g., Carslaw and Jaeger, 1959; deVries and Peck, 1958). The simplest approximation is to consider the cable as an infinitely long line source of infinitesimal radius Carslaw and Jaeger (1959), deVries and Peck (1958), Shiozawa and Campbell (1990), Bristow et al. (1994).

Analytical solutions also exist for the more realistic case of a cylindrical heat source covered by an insulating sheath and buried in a homogeneous isotropic medium (Carslaw and Jaeger, 1959). We will regard the cylindrical heat source of external radius a (m) as a perfect conductor of thermal capacity per unit cable length S (J m^{-1} K^{-1}) and we will assume that the insulation has negligible thermal capacity and thermal resistance per unit cable length R (K W^{-1} m^{-1}); the properties of the soil surrounding the cable are the thermal conductivity λ (W m^{-1} K^{-1}), the volumetric heat capacity C (Jm^{-3} K^{-1}), and the thermal diffusivity $K = \lambda/C$ (m^2 s^{-1}).

Assuming a constant heat source of strength Q (W m^{-1}) per unit cable length, the temperature increment with respect to the initial temperature is (Carslaw and Jaeger, 1959)

$$\Delta T(t) = T(t) - T(0) = \frac{Q}{\lambda} G(h,\beta,\tau), \quad [1]$$

where t is the elapsed time since the heating started,

$$h = 2\pi R\lambda, \quad [2]$$

$$\beta = 2\pi a^2 C/S, \quad [3]$$

$$\tau = Kt/a^2, \quad [4]$$

and

$$G(h,\beta,\tau) = \frac{2\beta^2}{\pi^3 C}\int_0^\infty \frac{1-\exp(-u^2\tau)}{u^3\Delta_1(h,\beta,u)}du, \quad [5]$$

with

$$\Delta_1(h,\beta,u) = [uJ_0(u)-(\beta-hu^2)J_1(u)]^2 + [uY_0(u)-(\beta-hu^2)Y_1(u)]^2, \quad [6]$$

where $J_n(u)$ and $Y_n(u)$ are the Bessel functions of order n of the first and second kind, respectively. For $\tau >> 1$, Eq. [1] can be written as,

$$\Delta T(t) = \frac{Q}{4\pi\lambda}\left[2h + \ln\frac{4\tau}{c} - \frac{(4h-\beta)}{2\beta\tau} + \frac{\beta-2}{2\beta\tau}\ln\frac{4\tau}{c} + \ldots\right] \quad [7]$$

where $c = 1.7811 = \exp\gamma$, and $\gamma = 0.5772\ldots$ is the Euler–Mascheroni constant. At the lowest order in τ and after some simple manipulations, we obtain

$$\Delta T(t) = \frac{Q}{4\pi\lambda}\left[\ln(t) + 2h + \ln\left(\frac{4K}{a^2 c}\right)\right], \quad [8]$$

which shows that the temperature increment depends logarithmically on time when $t >> a^2/K$ and that the effects of the insulating sheath do not affect the proportionality constant, $Q/4\pi\lambda$, which depends only on the heat source and on the thermal conductivity of the medium. Analogously to the classical Cooper–Jacob method for pumping-test interpretation (see, e.g., Bear, 1979), Eq. [8] allows estimating the thermal conductivity of the soil from the slope of the linear regression between the temperature increments, ΔT, and the logarithm of time, $\ln(t)$. Once the thermal conductivity has been estimated, the thermal diffusivity K can be obtained from the intercept of the linear regression if h and a are known; and from the diffusivity one can calculate the volumetric heat capacity, C. For a heat source of finite duration Δt_h, the problem can be divided into a heating phase, $0 < t < \Delta t_h$, in which the solution is again given by Eq. [1], and a cooling phase, $t > \Delta t_h$, in which the temperature increase can be written as a superposition of two solutions, one with positive and the other with a negative heat source, i.e.,

$$\Delta T(t) = \frac{Q}{\lambda}[G(h,\beta,\tau) - G(h,\beta,\tau-\Delta\tau_h)], \quad [9]$$

where $\Delta\tau_h = K\Delta t_h / a^2$ is the dimensionless heating time. The second term in Eq. [9] represents an imaginary cooling, which is necessary to obtain a zero heat source term after heating ceases. At later time, $t >> (a^2/K) + \Delta t_h$, $G(h,\beta,\tau)$ and $G(h,\beta,\tau-\Delta\tau_h)$ can be asymptotically expanded for large τ and $\tau - \Delta\tau_h$, respectively, which yields, at lowest order and after some manipulations,

$$\Delta T(t) = \frac{Q}{4\pi\lambda}\ln\left(\frac{t}{t-\Delta t_h}\right). \quad [10]$$

Equation [10] shows that the long-time analysis of the cooling phase allows the estimation of the thermal conductivity from the slope of the linear regression between ΔT and $\ln[t/(t-\Delta t_h)]$. The first neglected term is

$$\frac{Q}{4\pi\lambda}\Delta\tau\left[\frac{(4h-2)}{2\beta\tau^2} - \frac{\beta-2}{2\beta\tau^2}\ln\frac{4\tau}{c}\right]$$

which is proportional to $1/\tau^2$ and approaches zero faster than the first neglected term in Eq. [8], which is proportional to $1/\tau$ (see Eq. [7]). This indicates that the solution for the cooling approaches the asymptotic limit (Eq. [10]) more rapidly than the heating solution. We observe that this analysis does not allow estimating the heat capacity. If Eq. [8] and [10] are applied to pre-asymptotic data, the probe method leads to a systematic underestimation of the thermal conductivity (see, e.g., Bristow et al., 1994). Van der Held and Van Drunen (1949) have proven that this issue can be reduced by adding a time correction, t_0, to the argument of $\ln(t)$ in Eq. [8] which reduces the difference with the exact solution, Eq. [1], and allows improving the estimate of the thermal properties from non-asymptotic measurements. deVries (1952) applied a similar strategy to analyze data from a cooling event and added a time correction, t_0, in Eq. [10] obtaining

$$\Delta T(t) = \frac{Q}{4\pi\lambda}\ln\left(\frac{t+t_0}{t-\Delta t_h+t_0}\right). \quad [11]$$

Once t_0 is determined, the thermal conductivity can be inferred from the slope of the linear regression between ΔT and $\ln[(t+t_0)/(t-\Delta t_h+t_0)]$.

Estimation of the Water Content from the Thermal Conductivity

With the probe method presented in the previous section we have at our disposal two strategies to estimate the thermal conductivity from

the temperature response of the soil: one is based on the analysis of the heating phase and allows, in principle, also the estimation of the volumetric heat capacity; the other is based on the analysis of the cooling phase. As both the thermal conductivity and the volumetric heat capacity of the soil depend on the soil moisture, it is possible to infer the water content from the estimated thermal properties when reliable constitutive relationships are available. Despite the advantages of retrieving the soil moisture from the volumetric heat capacity (Bristow et al., 1993), an accurate estimate requires knowledge of the inner cable radius and of the thermal resistance of the insulator, and a sufficiently long heating time, which might perturb the soil state by providing a large amount of energy. More fundamentally, the exponential dependence of the heat capacity on the intercept of the linear regression requires an unrealistically precise estimate of the intercept to obtain reliable volumetric heat capacity. For these reasons, we concentrate on the use of the thermal conductivity to infer the water content.

Several constitutive relationships to describe the dependence of λ on the volumetric water content (from now on also indicated with θ) exist (see, e.g., Johansen, 1975; Chung and Horton, 1987; Côté and Konrad, 2005; Lu et al., 2007; Jougnot and Revil, 2010). Here we employ the model from (Lu et al., 2007) (Fig. 1) that expresses the thermal conductivity of moist soil as

$$\lambda = (\lambda_{sat} - \lambda_{dry}) Ke + \lambda_{dry} , \quad [12]$$

where λ_{dry} and λ_{sat} are the thermal conductivities of the dry and saturated soil, respectively:

$$K_e = \exp\left\{\alpha\left[1-\left(\frac{\theta}{\theta_{sat}}\right)^{(\alpha-1.33)}\right]\right\}, \quad [13]$$

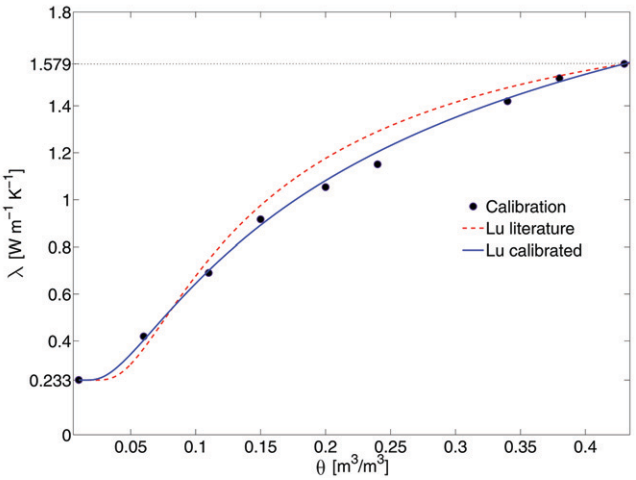

Fig. 1. Thermal conductivity (λ) as a function of the volumetric water content (θ) according to model from Lu et al. (2007). The black dots represent the points acquired in laboratory using the Multi-Function Heat Pulse Probes. The blue dashed line is the curve with the standard value α from Lu et al. (2007) for fine soils. The solid line is the best fit of the black dots, with parameter α_{Fit}. The values of θ_{sat}, θ_{res}, λ_{sat}, λ_{dry}, α, and α_{Fit} are listed in Table 1.

is the Kersten number (Johansen, 1975); θ_{sat} the saturated volumetric water content; and α a parameter that depends on the soil texture.

Error Analysis

Inferring θ from the temperature response to heating involves two steps: the first requires the estimation of λ from the analysis of the temperature increment as a function of time; the second requires the use of constitutive relationships linking λ to θ. To assess the accuracy of the measurements it is important to quantify how the errors propagate from the estimated linear-regression parameters to θ. Given a linear relationship between ΔT and $\ln(t)$, $\ln[t/(t-\Delta t_h)]$ or $\ln[(t+t_0)/(t+t_0-\Delta t_h)]$, a simple linear regression provides the parameters m and b (the slope and the intercept, respectively) of the straight line that minimizes the sum of the squared residuals. Assuming a negligible error on the time, the variance of the measured temperature increments is

$$\sigma^2 = \frac{1}{N-2}\sum_{i=1}^{N}\left[mx_i + b - \Delta T_i\right]^2, \quad [14]$$

where the subscript i denotes the ith measurement, and $x_i = \ln(t_i)$ for the analysis of the heating phase, $x_i = \ln[t_i/(t_i - \Delta t_h)]$ and $x_i = \ln[(t_i + t_0)/(t_i + t_0 - \Delta t_h)]$ for the analysis of the cooling phase with and without time correction t_0, respectively. The uncertainty on the slope and the intercept is obtained by propagating the uncertainty on the temperature increments, which yields

$$\sigma_m^2 = \frac{N}{\Delta}\sigma^2, \quad [15]$$

and

$$\sigma_b^2 = \frac{\sum_{i=1}^{N} x_i^2}{\Delta}\sigma^2, \quad [16]$$

respectively, with

$$\Delta = N\sum_{i=1}^{N} x_i^2 - \left[\sum_{i=1}^{N} x_i\right]^2 . \quad 17]$$

Propagating the uncertainty to thermal conductivity we obtain

$$\frac{\sigma_\lambda^2}{\lambda^2} = \frac{\sigma_m^2}{m^2} + \frac{\sigma_Q^2}{Q^2}, \quad [18]$$

which shows that the relative error on the thermal conductivity is simply equal to the relative error on the slope, when the relative error on the heat-source strength σ_Q/Q is negligible. On the other hand, the relative uncertainty on the volumetric heat capacity calculated by standard error propagation through Eq. [8], (see, e.g., Taylor, 1997) is

$$\frac{\sigma_C^2}{C^2} = (1+4\pi\lambda R)^2 \frac{\sigma_\lambda^2}{\lambda^2} + \frac{b^2}{m^2}\left(\frac{\sigma_m^2}{m^2}+\frac{\sigma_b^2}{b^2}\right) + 4\frac{\sigma_a^2}{a^2} + (4\pi\lambda R)^2 \frac{\sigma_R^2}{R^2}, \quad [19]$$

which is always larger than the relative error on λ. Notice that the relative variances of the slope and the intercept are amplified by a factor $(b/m)^2$. The exponential dependence on the ratio b/m, as given by Eq. [8], brings this term to be a multiplier of the uncertainty, unavoidably leading to large errors whenever the ratio is not small. Moreover, an accurate estimate of C requires an accurate measurement of the (small) external source radius, a, and of the thermal resistance of the insulator, R. Propagation of σ_λ through Eq. [13] provides the uncertainty σ_θ on the retrieved values of θ. Assuming unaffected by error the values of λ_{dry} and λ_{sat}, the error on the volumetric water content is

$$\sigma_\theta = \left|\frac{dK_e}{d\theta}\right|^{-1} \sigma_{K_e} = \left|\frac{dK_e}{d\theta}\right|^{-1} \frac{\sigma_\lambda}{\lambda_{sat}-\lambda_{dry}} = \left|\frac{d\lambda}{d\theta}\right|^{-1} \sigma_\lambda, \quad [20]$$

which shows that the error on λ is amplified in regions of large water content, where $d\lambda/d\theta$ is small.

Experimental Setup

The Lysimeter and the Soil

The deployment of a fiber optic cable has been performed in a weighable lysimeter at EPFL (Fig. 2). The lysimeter, a polyester tank of height 2.50 m and diameter 1.20 m, is placed on three high-accuracy loading cells (not used in this work). The top of the lysimeter is flush with the surrounding soil surface and exposed to meteorological forcing. The bottom of the lysimeter has been prepared with a filter consisting of 0.25 m of gravel topped with 0.25 m of coarse sand. The remaining 2 m have been filled with an alluvial loam from Conthey, VS, in southern Switzerland. To obtain as homogenous as possible packing, the lysimeter was filled through successive steps each involving a gentle deposition of soil followed by several saturation-drainage cycles in an attempt to achieve ideal settling. During the filling, the lysimeter was equipped with nine capacitance-based 5TM probes (Decagon Device Inc.) and nine type T (copper-constantan) thermocouples, which were placed in the soil at the nine different depths (see Fig. 2). Data were collected every 60 s by a Campbell CR5000 datalogger for the 5TM probes and by a solid state multiplexer for thermocouples (Campbell AM25T) and directly transferred to a PC installed in the basement. Several soil samples were taken to determine particle size distribution, bulk density, porosity, and residual water saturation (Table 1). The dry-soil, λ_{dry}, and saturated soil, λ_{sat}, thermal conductivity were measured in small samples filled with oven-dried and saturated soil, respectively, by means of two five-needles multifunction heat pulse probes (MFHPP) (Mori et al., 2003; Kamai et al., 2008); the measured values are in good agreement with the values reported by Lu et al. (2007) for a similar type of loam. Independent measurements of λ at different soil saturations were also obtained with the same technique employed for λ_{dry} and λ_{sat}. A calibrated Lu model was obtained by fitting the experimental data with the free parameter α_{Fit} and values λ_{dry} and λ_{sat} from the laboratory measurements. In Fig. 1, the calibrated Lu curve is compared with a curve employing the standard value of α for fine soils from Lu et al. (2007). The similarity between Conthey loam and fine-textured soils is due to the high fraction of fine particles (smaller than 200 μm) and the low bulk density, which is much closer to silt and clay than to pure sand (see, e.g., Lu et al., 2007). We observe small difference between the two curves at medium water contents [between 0.2 and 0.3 ($m^3\ m^{-3}$)], where the inferred θ can differ by 0.04 ($m^3\ m^{-3}$) depending on the curve employed. This suggests that Lu's model with standard values of α provides a good approximation and can be used to estimate the water content

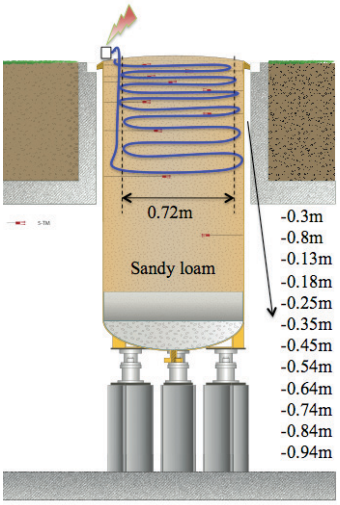

Fig. 2. The EPFL weighable lysimeter has been equipped with several sensors during the campaign of summer 2010. The optical fiber (sketched with a blue line) is installed in the lysimeter forming nine loops at approximate depth indicated in the drawing. To obtained independent volumetric water content measurements, 5TM probes (represented by small prongs) are also installed in the lysimeter at depths 0.3, 0.8, 0.13, 0.18, 0.25, 0.35, 0.45, 0.60, and 1 m.

Table 1. Properties of the loam (from Conthey, VS, southern Switzerland).

Property†	Value	Unit
Coarse sand (200–2000 μm)	17‡	%
Fine sand (50–200 μm)	38‡	%
Coarse silt (20–50 μm)	18.3‡	%
Fine silt (2–20 μm)	16.7‡	%
Clay (<2 μm]	10‡	%
θ_{sat}	0.43‡	[$m^3\ m^{-3}$]
θ_{res}	0.08‡	[$m^3\ m^{-3}$]
ρ_b	1.3‡	[$kg\ m^{-3}$]
λ_{dry}	0.233§	[$W\ m^{-1}\ K^{-1}$]
λ_{sat}	1.579§	[$W\ m^{-1}\ K^{-1}$]
α	0.27¶	[–]
α_{Fit}	0.67§	[–]

† Subscripts: sat, saturation value; res, residual value; dry, dry value; Fit, fitted value.
‡ Laboratory granulometric analysis.
§ Laboratory tests with heat pulse probes.
¶ Lu et al. (2007).

with a reasonable accuracy in cases where a specific calibration of the model is not available. All soil parameters relevant for this study are summarized in Table 1.

DTS and Optical Fiber

The optical fiber was installed during the lysimeter filling. The cable used (BRUsteel from Brugg Cable) consists of a stainless steel loose tube containing four multimode 50 μm cores and 125 μm cladding fibers; it is armored with an outer sheath of interlaced metal wires, which guarantees flexibility and high protection in outdoor applications, and covered by a polyamide jacket for thermal and electrical insulation. The external cable diameter is 3.8 mm and the total cable length is 280 m. Figure 3 shows the different layers characterizing the composite structure of the fiber cable. The fiber optic cable is connected to a DTS ORYX (Sensornet Inc.) which employs a laser pulse time of 10 ns corresponding to a spatial resolution of 1 m, and acquires measurements at a frequency of 1/15 Hz. About 32-m of fiber optic cable were buried in the lysimeter during the filling starting at from depth of 0.94 m from the surface. The cable was installed in a long spiral consisting of twelve rings of approximate diameter 0.72 m; the vertical distance between rings decreases approaching the surface as sketched in Fig. 2. To preserve the shape and the depth of the spiral, the fiber has been wound around some thin bamboo sticks that were temporarily inserted in the soil and removed at the end of the filling (see Fig. 4). This technique avoided the presence of a permanent rigid structure in the lysimeter that could potentially disturb the packing, but the lack of anchorage left the fiber and the probes free to move during the natural settling that unavoidably occurred with time and exposure to meteorological conditions (rainfall, wind, evaporation). Since a subsidence of about 0.05 m was observed during the 3 mo between the end of the filling and the experiments, a depth uncertainty of about 0.02 m can be realistically estimated with respect to the value reported in Fig. 2. Before entering and after exiting the soil, the cable was immersed in two calibrating baths placed in the basement: a cold bath consisting of ice at temperature −0.4°C and a warm bath consisting of water mixed through an aquarium bubbler and kept at 21°C by a thermistor. The temperatures of the baths were monitored by two PT100 (Campbell Sci.) and the averaged temperature recorded over the entire duration of the experiment (about 24 h) was used to calibrate the optical fiber. The use of cold and hot baths allowed calibrating both the offset and the slope. We have observed a deterioration of the declared sensitivity of the DTS ORYX (0.1°C), which has been estimated of the order of ±0.4°C based on the temperature fluctuations in the calibrating baths (see Fig. 5). This sensitivity loss can be due, for instance, to slight differences in the vibrational energy between the molecules that cause a broadening of the Stokes and Anti-Stokes Raman peaks; to the differential attenuation that leads to changes in the input-output intensity ratio; or to the intensity loss in the transmission due to the splicing between the connectors and the fibers.

Fig. 3. The BRUsteel cable. From left to right: the nylon jacket (1), the inter-laced steel wires (2), the stainless steel loose tube (3), the four multimode fibers (4). In (3) is applied the electrical heating. From Brugg Cables (http://www.bruggcables.com), technical sheet of the BRUsteel fiber cable.

Fig. 4. Installation of the fiber optic cable. During uniform packing of the lysimeter, the soil is saturated and the fiber optic cable is wrapped around a bamboo-stick structure, which is removed after filling.

Fiber Heating and Probe-Method Measurements

To generate the heat source necessary for the probe method, the metal sheath was heated allowing an electric current to flow through the buried portion of the cable. A few centimeters of the Polyamide cover were removed at the two points immediately outside the soil; two small battery clamps were fixed to the uncovered metal sheath of the BRUsteel and plugged to the domestic electric network at 230 VAC. To avoid shock risks, the clamps were put in two boxes for electric cable filled with foam for thermal insulation. To reduce both the applied voltage and the current intensity along the sheath, a power consumer with two regulations was connected to the circuit. A switch allowed the electric current to start/stop, while a Voltmeter and an Amperometer monitored voltage and current intensity, respectively. Of the six heating events performed over a 24-h period (from the afternoon of 28 October through the morning of 29 Oct. 2010), three had an electrical voltage of 63 V and three a more intense voltage of 115.6 V. Since the measured resistance of the metal sheath is 0.365 Ω m^{-1}, the dissipated power can be calculated to be about 11 W m^{-1} and 36 W m^{-1} for the low and high voltage events, respectively. These powers are of the same order of magnitude as those applied by Weiss (2003) and Sayde et

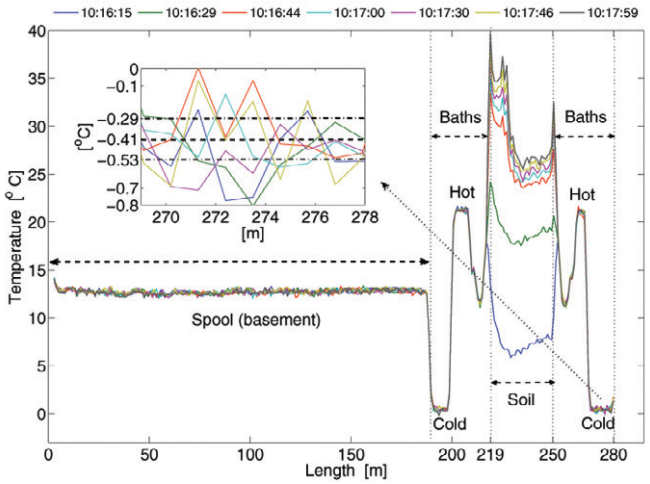

Fig. 5. Temperature profiles measured by the optical fiber during a heating pulse. The subplot shows the temperature in the cold bath which displays fluctuations on the order of ± 0.4°C around the mean value of −0.41°C (dashed line, measured with PT100 probe ± standard deviation over the entire experiments duration).

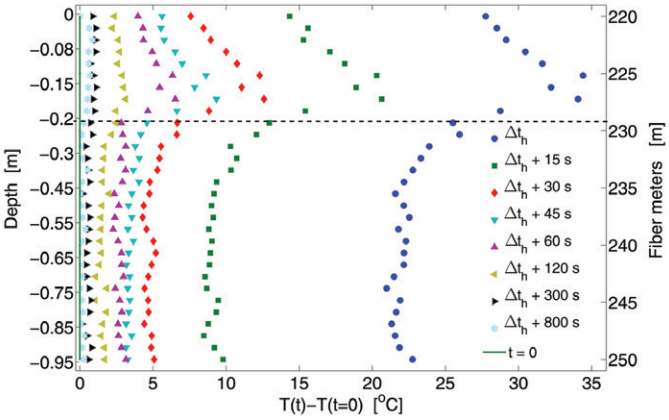

Fig. 6. Temperature increments, $T(t) - T\ (t = 0)$, measured by the fiber optic cable during cooling (heat pulse stopped at Δt_h = 120 s). The dashed line highlights the interface between two zones showing different responses to the heat pulses: in the shallower zone (approximately the initial 9 m of the buried fiber) temperature sensitively increases during heating, whereas the deeper zone shows a limited temperature increment.

al. (2010), i.e., 20 W m^{-1}. All heating events lasted Δt_h = (120 ± 1) s and were followed by long cooling periods.

Results

Temperature Measurements during Heating and Cooling

The temperature profile along the whole fiber optic cable length is shown in Fig. 5 for several times during one of the heating events. From the profile, the calibrating baths are clearly visible, and it is possible to identify the heated portion of the cable as the section between the lengths 219 m and 250 m. Due to the partial burial of the fiber optic cable, the two extreme values of this portion are excluded from the following data analysis. The length of the fiber considered is therefore 30 m (larger fiber-length values correspond to deeper soil). In this section, the temperature response of the soil to the heating is clearly visible, and shows a more rapid increase and larger temperature increments close to the surface. This indicates a lower thermal conductivity near the surface, which is consistent with the typically lower volumetric water content of the shallower soil. An example of measured temperature-increment profiles along the buried section of the fiber optic cable during cooling is shown in Fig. 6. As in the heating phase, the shallow soil displays a reduced ability to transfer heat and the temperature relaxation to its value before heating is slower. Compared to the heating phase which has a duration of 120 s, the cooling phase is longer 300 s after heating stopped the temperature-increment is still well-visible. After 800 s, the temperature-increment reduces to zero almost everywhere, except close to the surface where a small positive increment is detectable. The temperature increments observed during our experiments were of the same magnitude as those measured in other studies (e.g., Weiss, 2003 and Sayde et al., 2010). Note that the temperature measured by the optical fiber during heating and cooling is not the temperature of the soil. Due to the presence of the polyamide jacket, which acts as an insulation layer (see Estimation of Thermal Properties by the Probe Method), the actual temperature increment in the soil is smaller and it is unlikely that it can induce rapid water redistribution around the fiber optic cable.

Determination of the Thermal Properties by the Probe Method

The soil-temperature response to the heat pulse is used to determine the thermal properties of the soil. The probe method can be applied both to the heating and the cooling phase by employing the asymptotic solutions for late time (Eq. [8] and [10], respectively). For the data collected in this experiment, a tentative analysis of the heating phase showed that the duration Δt_h = 120 s was too short to approach the asymptotic solution. This was verified by plotting $\Delta T(t_i) - \Delta T(t_{i-1})/\ln(t_i) - \ln(t_{i-1})$ as a function of $\ln(t_i)$ for all the times t_i at which temperature measurements were available (seven per heating event). This diagnostic plot (not presented here) showed that this quantity was decreasing during the entire heating phase, which indicates that the asymptotic solution was not approached within 120 s. In contrast to the heating phase, the cooling phase offers the advantage of longer duration and more rapid approach to the asymptotic solution (see the discussion at the end of Estimation of Thermal Properties by the Probe Method, which shows how the first term neglected is order $\ln\tau/\tau^2$ instead of order $\ln\tau/\tau$). On the other hand, the signal-to-noise ratio tends to decrease at later time, such that the first point to be included in the linear regression to estimate the thermal conductivity has to be carefully chosen. The diagnostic plot employed for the heating phase is not effective for the cooling phase because the differences

between temperature increments become very small for $t >> \Delta t_h$ due to the unfavorable signal/noise ratio. To verify the degrees of accuracy of the asymptotic approximation, we compare the thermal conductivity values obtained considering only temperature increments measured after a threshold time, $t_{thr} > \Delta t_h$. By increasing the threshold, the estimated values of thermal conductivity tend to the asymptotic value, whereas the uncertainty increases due to the fewer data points employed and, most importantly, to the deterioration of the signal/noise ratio. The diagnostic plots for the linear regressions of the three cooling events yielded similar results and revealed a good repeatability of the experiment, which is a direct consequence of the minor water-content variations over the entire period. As the three cooling events yielded statistically consistent estimates, we decided to perform a simultaneous linear regression of all data, which allows a significant reduction of the statistical uncertainty by increasing the number of data points. All the results presented in the remainder of the paper are obtained by simultaneous analysis of the three cooling events. Figure 7 shows the diagnostic plot from simultaneous linear regression of the three cooling events. The thermal conductivity is plotted as a function of the threshold time (i.e., as a function of the time from which temperature increments are included in the linear regression) for two representative meters of fiber, one close to the surface and the other close to the bottom of the spiral of fiber optic cable. For both fiber intervals, the estimated thermal conductivities initially grow when the threshold time is increased, which indicates that the temperature increment is not yet asymptotic and that the thermal conductivity is systematically underestimated. After a certain threshold time, the estimated thermal conductivities remain constant within statistical uncertainty. The threshold after which the estimated λ values remain constant is the optimal starting point, because it is consistent with the assumption that the solution is

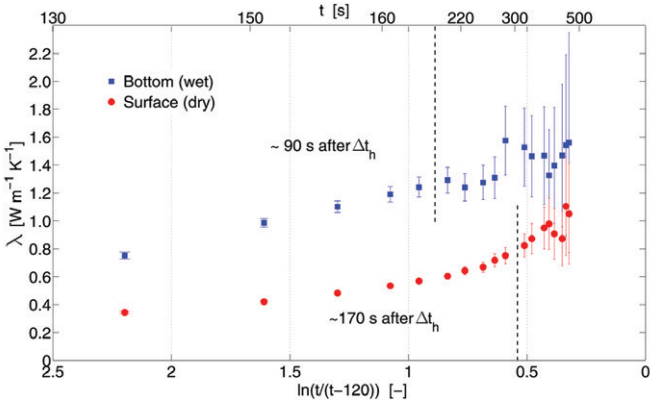

Fig. 7. Diagnostic plots of two representative sections of the optical fiber: one at the bottom of the coil (meter 248, blue), the other close to the surface (meter 226, red). The thermal conductivity is plotted as a function of the time from which temperature increments are included in the linear regression. Shown are the results for three cooling events considered together. The dashed vertical lines indicate the time after which the estimated thermal conductivities are consistent within statistical uncertainty (i.e., 90 s for the deeper and 170 s for the shallower fiber section, respectively).

asymptotic and allows to minimize the uncertainty propagation to the slope which tends to rapidly grow if the threshold is raised further. Indeed, as it is evident from the error analysis in Error Analysis, the points characterized by larger $x_i = \ln[t_i/(t_i - \Delta t_h)]$ are more effective in reducing the propagation of the variance of the measured temperature increments to the uncertainty of m (Eq. [15] and [17]); in contrast the use of points characterized by small $x_i = \ln[t_i/(t_i - \Delta t_h)]$ leads to small Δ (Eq. [17]). (Note that a smaller slope uncertainty does not necessarily mean that the hypothesis of linear dependence is better satisfied, as it is evident from Fig. 7). The threshold values are 170 s and 90 s for the shallower and the deeper fiber meter, respectively. The different thresholds for the shallower and deeper measurements is due to the fact that, for the solution to be asymptotic, we have to require that $t - \Delta t_h >> a^2 c/\lambda$, and shallower soil is drier and has lower λ. According to the results of the diagnostic plot, Fig. 7, and to account for the difference between dry and wet soil, we have chosen a threshold of 170 s for the first 9 m of optica fiber (in dryer soil) and a threshold of 90 s for the remaining part of the fiber. The estimated thermal conductivities are plotted in Fig. 8 (blue squares) as a function of the fiber length and show an abrupt transition from a region of lower to a region of higher thermal conductivity around the 0.2-m depth.

Determination of Thermal Properties with Time Correction

If the asymptotic limit of Eq. [9] is not yet reached, the analysis above leads to a systematic underestimation of the thermal conductivity as it can be clearly observed from Fig. 7. Since the diagnostic plot suggests that the data are not yet strictly asymptotic, we repeat the analysis introducing a time correction, t_0, in Eq. [11] (Van der Held and Van Drunen, 1949; deVries, 1952). The standard method to infer t_0, which is based on an analysis of the increment ratio $\Delta t/\Delta T$ (see, e.g., Van der Held and Van Drunen, 1949), has proven inapplicable to our data due to the large fluctuations of the increment ratio at later time. Therefore, we proceed differently and perform a nonlinear regression of ΔT as function of t with two free parameters, t_0 and λ. (For this purpose we have used the nonlinear-regression package cftool of MATLAB; http://www.mathworks.ch/help/toolbox/curvefit/cftool.html; accessed February 2012). The uncertainty on λ (indicated by the error bars in Fig. 8) is calculated from the equations presented in the Error Analysis section assuming that the uncertainty on t_0 can be neglected. As for the case without time correction, we determine the optimal threshold time from a diagnostic plot analogous to the one in Fig. 7. The threshold time, t_{thr}, is determined independently for each meter of the optical fiber and varies between 45 s and 100 s in shallower soil (above the abrupt transition in thermal conductivity), and between 15 s and 45 s in deeper soil. The values of t_0 are all negative and range from −26 to −66 s close to the surface, and from −12 to −24 s toward the bottom of the fiber optic cable coil. Note that these threshold times are significantly shorter than those from the analysis without t_0, indicating that earlier data can be employed to obtain an accurate estimate of the thermal

conductivity. Negative values of the time correction, t_0, in Eq. [11] have also been found in previous studies (e.g., Van der Held and Van Drunen (1949) and Bristow et al. (1994)) and confirm that the data analyzed are not yet asymptotic. More negative values close to the surface indicate that in dry conditions the asymptotic regime is reached later than in wet conditions, when the time corrections are closer to zero. The results of this analysis are plotted in Fig. 8 and show that the estimated thermal conductivity is systematically larger and the statistical error significantly reduced compared to the results obtained without time correction.

Estimate of the Volumetric Water Content

According to the constitutive relationships in Fig. 1, the variation of thermal conductivity along the fiber indicates the presence of a variably wetted soil (under the assumption of constant soil texture and bulk density), with a clear distinction between the drier zone around the initial nine meters of fiber optic cable (shallower soil) and the wetter zone (deeper soil). The volumetric water contents obtained by inverting the calibrated Lu's model (solid line in Fig. 1) are presented in Fig. 9 as a function of the fiber depth, which has been estimated from the geometry of the coil. The error bars indicate the error propagation obtained from Eq. [20]. The error on θ is smaller in the dryer region, grows in the wet region, and exhibits a maximum at about 0.54 to 0.58 m from the surface for both cases. This larger error is due to the dependence of σ_θ on $|dK_e/d\theta|^{-1}$ (Eq. [20]) which amplifies the uncertainty in a region where the constitutive relationship is rather flat. In Fig. 9 the results obtained both with and without time correction are compared with the volumetric water contents independently measured by nine 5TM probes. The analysis without time correction t_0 yields a systematic underestimation of the water content, whereas the agreement between DTS and 5TM probes is substantially improved when t_0 is introduced. In particular, between 0.2 and 1 m the agreement is excellent, with an accuracy of 0.04 ($m^3\ m^{-3}$) in the worst case at the 0.6-m depth. At depths shallower than 0.2 m, both analysis (with and without time correction) noticeably underestimate the volumetric water content.

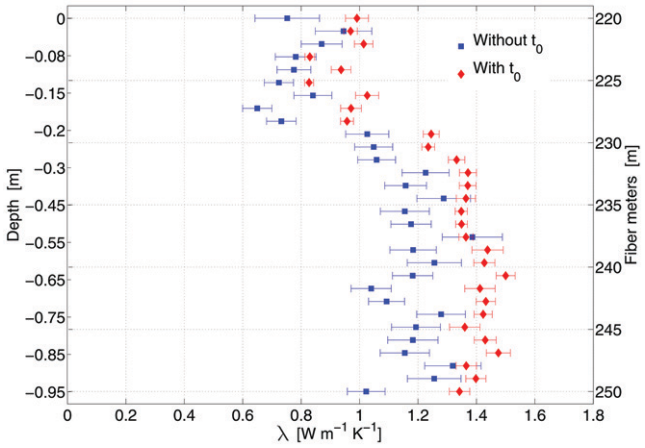

Fig. 8. Estimated thermal conductivities as a function of the fiber length in the case with time correction t_0 (red diamonds) and without (blue squares).

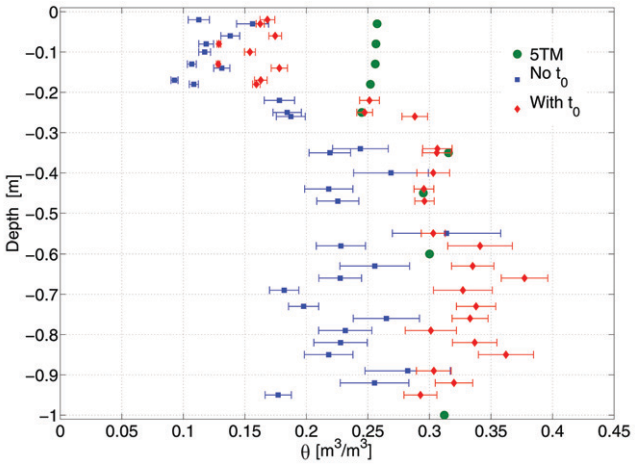

Fig. 9. Volumetric water contents at different depths estimated from thermal conductivities by inversion of the Lu et al. (2007) model with calibrated parameter α_{Fit} for the case of λ inferred with t_0 (diamonds) and without (squares). Circles represent the independent 5TM measurements.

Conclusions

Through analysis of the cooling phase of a heated optical fiber we have estimated the thermal conductivity of the soil and inferred the volumetric water content. The approach relies on the use of asymptotic solutions for the propagation of heat and on the availability of reliable models (Lu et al., 2007) to relate thermal conductivity and soil moisture. Comparison with independent measurements of soil moisture (obtained using 5TM probes) demonstrated that AHFO measurements underestimate the water content in drier soils. This is due to the longer time required for the temperature increment to become asymptotic in poorly conductive media. In wetter soils, however, the estimation of volumetric water content was excellent. In this region, the introduction of a time correction allows to reduce the statistical uncertainty of volumetric water content measurements below 0.02 ($m^3\ m^{-3}$). For future application of the AHFO method, there are areas for improvement. One should make use of longer heating and cooling events to allow a more sound application of the asymptotic solutions to the temperature-increment evolution in dry soils. Note that the asymptotic analysis offers the advantage of not requiring one to account for the effects of the polyamide insulator. The BRUsteel cable consists of a central steel loose tube protected by steel interlaced wires and by 0.3 mm of nylon jacket. The effect of this composite structure has been clearly observed at early time when the measured temperature increment was uniform along the entire cable and influences the behavior of pre-asymptotic temperature increments. To reduce the statistical uncertainty of the method and the error propagation on the estimated volumetric water content ideally more data points should be used in the linear regression. This can be addressed in practice by allowing for longer heating and cooling phases and making use of DTS devices that measure with higher frequency

than the one employed in the present study. The results presented here are very encouraging and demonstrate that the error can be reduced and a good estimate of volumetric water content can be obtained in wet soils by employing a time correction. Future studies should allow for longer heat pulses to improve the signal/noise ratio. This will also require an assessment of the effects of larger heat supply on soil water redistribution.

Acknowledgments

The authors are grateful to the reviewers for the helpful suggestions which greatly improved the quality of the manuscript. Special thanks are also addressed to J. Golay, F. Comino, M. Froidevaux and S. Varun (EPFL), D. Jougnot (University of Lausanne) and K. Hilgersom (TU Delft) for their precious collaboration. This work was founded by the Swiss National Science Foundation (200021-1222088/1). Ivan Lunati is a Swiss National Science Foundation (SNSF) Professor at the University of Lausanne (supported by the SNSF grant number PP00P2-123419/1).

References

Assouline, S., K. Narkis, S.W. Tyler, I. Lunati, M.B. Parlange, and J.S. Selker. 2010. On the diurnal soil water content dynamics during evaporation using dielectric methods. Vadose Zone J. 9:709–718. doi:10.2136/vzj2009.0109

Auñeger, M., M. Conrad, S. Perzlmaier, and P. Porras. 2005. Improving a fiber optics tool for monitoring leakage. Hydro Rev. Worldwide 13:18–23.

Bear, J. 1979. Hydraulics of groundwater. Dover, New York. p. 467–472.

Bristow, K.L., G.S. Campbell, and C. Calissendorff. 1993. Test of a heat pulse probe for measuring changes in soil water content. Soil Sci. Soc. Am. J. 57:930–934. doi:10.2136/sssaj1993.03615995005700040008x

Bristow, K.L., R.D. White, and G.J. Kluitenberg. 1994. Comparison of single and dual probes for measuring soil thermal properties with transient heating. Aust. J. Soil Res. 32:447–464. doi:10.1071/SR9940447

Campbell, J.E. 1990. Dielectric-properties and influence of conductivity in soils at one to 50 MHz. Soil Sci. Soc. Am. J. 54(2): 332–341. doi:10.2136/sssaj1990.03615995005400020006x

Carslaw, H.S., and J.C. Jaeger. 1959. Conduction of heat in solids. 2nd ed. Clarendon Press, Oxford, UK.

Chung, S.O., and R. Horton. 1987. Soil heat and water flow with a partial surface mulch. Water Resour. Res. 23(12):2175–2186. doi:10.1029/WR023i012p02175

Côté, C., and J.-M. Konrad. 2005. A generalized thermal conductivity model for soils and construction materials. Can. Geotech. J. 42:443–458. doi:10.1139/t04-106

de Vries, D.A. 1952. A nonstationary method for determining thermal conductivity of soil in situ. Soil Sci. 73:83–90 . doi:10.1097/00010694-195202000-00001

de Vries, D.A., and A.J. Peck. 1958. On the cylindrical probe method of measuring thermal conductivity with special reference to soils. Part 1. Extension of theory and discussion of probe characteristics. Aust. J. Phys. 11:255–271. doi:10.1071/PH580255

Freifeld, B.M., S. Finsterle, T.C. Onstott, P. Toole, and M. Pratt. 2008. Ground surface temperature reconstructions: Using in situ estimates for thermal conductivity acquired with a fiber optic distributed thermal perturbation sensor. Geophys. Res. Lett. 35:L14309. doi:10.1029/2008GL034762

Gratton, K.T.V., and B.T. Meggitt. 2000. Optical fiber sensor technology. Kluwer Academic Publishers, Boston, MA.

Hopmans, J.W., J.M.H. Hendrickx, and J.S. Selker. 1999. Emerging measurement techniques for vadose zone characterization. In M.B. Parlange and J.W. Hopmans, editors, Vadose zone hydrology: Cutting across disciplines. Oxford Univ. Press, New York. p. 279–316.

Johansen, O. 1975. Thermal conductivity of soils. Ph.D. diss. Norwegian Univ. of Science and Technol., Trondheim (CRREL draft transl. 637).

Jones, S.B., and D. Or. 2004. Frequency domain analysis for extending time domain reñectometry water content measurement in highly saline soils. Soil Sci. Soc. Am. J. 68(5):1568–1577.

Jougnot, D., and A. Revil. 2010. Thermal conductivity of unsaturated clay-rocks. Hydrol. Earth Syst. Sci. 14:91–98. doi:10.5194/hess-14-91-2010

Kamai, T., A. Tuli, G.J. Kluitenberg, and J.W. Hopmans. 2008. Soil water ñux density measure-ments near 1cmd−1 using an improved heat pulse probe design. Water Resour. Res. 44:W00D14. doi:10.1029/2008WR007036

Keller, C.A., H. Huwald, M.K. Vollmer, A. Wenger, M. Hill, M.B. Parlange, and S. Reimann. 2011. Fiber optic distributed temperature sensing for the determination of the nocturnal atmospheric boundary layer height Atmos. Meas. Tech. 4:143–149.

Lu, S., T. Ren, Y. Gong, and R. Horton. 2007. An improved model for predicting soil thermal conductivity from water content at room temperature. Soil Sci. Soc. Am. J. 71:8–14. doi:10.2136/sssaj2006.0041

Mohamed, S.O., P. Bertuzzi, A. Bruand, L. Raison, and L. Bruckler. 1997. Field evaluation and error analysis of soil water content measurement using the capacitance probe method. Soil Sci. Soc. Am. J. 61:399–408. doi:10.2136/sssaj1997.03615995006100020006x

Mori, Y., J.W. Hopmans, A.P. Mortensen, and G.J. Kluitenberg. 2003. Multifunctional heat pulse probe for the simultaneous measurement of soil water content, solute concentration, and heat transport parameters. Vadose Zone J. 2(4):561–571 10.2113/2.4.561.

Nadler, A., and Y. Lapid. 1996. An improved capacitance sensor for in situ monitoring of soil moisture. Aust. J. Soil Res. 34:361–368. doi:10.1071/SR9960361

Perzlmaier, S., M. Auñeger, and M. Conrad. 2004. Distributed fiber optic temperature measurements in hydraulic engineering- Prospects of the heat-up method. Proceedings of the 72nd ICOLD Annual Meeting Workshop on Dam Safety Problems and Solutions-Sharing Experience, Korean Natl. Comm. on Large Dams, 16–22 May, Seoul, Korea.

Perzlmaier, S., K.H. Straer, T. Strobl, and M. Auñeger. 2006. Integral seepage monitoring on open channel embankment dams by the DFOT heat pulse method. Proceedings of the 74th Annual Meeting, Int. Comm. on Large Dams, Barcelona, Spain.

Robinson, D.A., S.B. Jones, J.A. Wraith, D. Or, and S.P. Firedmena. 2003. A review of advances in dielectric and electrical conductivity measurements in soils using time domain reflectometry. Vadose Zone J. 2:444–475.

Robinson, D.A., C.S. Campbell, J.W. Hopmans, B.K. Hornbuckle, S.B. Jones, R. Knight, F. Ogden, J. Selker, and O. Wendroth. 2008. Soil moisture measurement for ecological and hydrological watershed-scale observatories: A review. Vadose Zone J. 7:358–389. doi:10.2136/vzj2007.0143

Sayde, C., C. Gregory, M. Gil-Rodriguez, N. Tufillaro, S.W. Tyler, N.C. van de Giesen, M. English, R. Cuenca, and J.S. Selker. 2010. Feasibility of soil moisture monitoring with heated fiber optics. Water Resour. Res. 46:W06201. doi:10.1029/2009WR007846

Steele-Dunne, S.C., M.M. Rutten, D.M. Krzeminska, M. Hausner, S.W. Tyler, J.S. Selker, T.A. Bogaard, and N.C. van de Giesen. 2010. Feasibility of soil moisture estimation using passive distributed temperature sensing. Water Resour. Res. 46:W03534.doi:10.1029/2009WR008272

Selker, J., N. van de Giesen, M. Westhoff, W. Luxemburg, and M.B. Parlange. 2006a. Fiber optics opens window on stream dynamics. Geophys. Res. Lett. 33:L24401.doi:10.1029/2006GL027979

Selker, J., L. Thevenaz, H. Huwald, A. Mallet, W. Luxemburg, N. van de Giesen, M. Stejskal, J. Zeman, M. Westhoff, and M.B. Parlange. 2006b. Distributed fiber optic temperature sensing for hydrologic systems. Water Resour. Res. 42:W12202.doi:10.1029/2006WR005326

Seyfried, M.S., and M.D. Murdock. 2001. Response of a new soil water sensor to variable soil, water content, and temperature. Soil Sci. Soc. Am. J. 65:28–34. doi:10.2136/sssaj2001.65128x

Seyfried, M.S., and M.D. Murdock. 2004. Measurement of soil water content with a 50 MHz soil dielectric sensor. Soil Sci. Soc. Am. J. 68:394–403. doi:10.2136/sssaj2004.0394

Shiozawa, S., and G.S. Campbell. 1990. Soil thermal conductivity. Remote Sens. Rev. 5:301–310. doi:10.1080/02757259009532137

Taylor, J.R. 1997. An introduction to error analysis. Oxford Univ. Press, Oxford, UK. p. 40–74.

Topp, G.C., S. Zegelin, and I. White. 2000. Impacts of the real and imaginary components of relative permittivity on time domain reflectometry measurements in soils. Soil Sci. Soc. Am. J. 64:1244–1252. doi:10.2136/sssaj2000.6441244x

Topp, G.C., J.L. Davis, and A.P. Annan. 1980. Electromagnetic determination of soil water content: Measurement in coaxial transmission lines. Water Resour. Res. 16:574–582. doi:10.1029/WR016i003p00574

Tyler, S., S. Burak, J. McNamara, A. Lamontagne, J. Dozier, and J. Selker. 2008. Spatially distributed temperatures at the base of two mountain snowpacks measured with fiber optic sensors. J. Glaciol. 54(187):673–679. doi:10.3189/002214308786570827

Tyler, S.W., J.S. Selker, M.B. Hausner, C.E. Hatch, T. Torgersen, C.E. Thodal, and G. Schladow. 2009. Environmental temperature sensing using Raman spectra DTS fiber optic methods. Water Resour. Res. 45:W00D23. doi:10.1029/2008WR007052

Van der Held, E.F.M., and F.G. Van Drunen. 1949. A method of measuring the thermal conductivity of liquids. Physica 15(10):865–881. doi:10.1016/0031-8914(49)90129-9

Vercauteren, N., H. Huwald, E. Bou-Zeid, J.S. Selker, U. Lemmin, M.B. Parlange, and I. Lunati. 2011. Evolution of superficial lake water temperature profile under diurnal radiative forcing. Water Resour. Res. 47:W09522. doi:10.1029/2011WR010529

Weiss, J.D. 2003. Using fiber optics to detect moisture intrusion into a landfill cap consisting of a vegetative soil barrier. J. Air Waste Manage. Assoc. 53:1130–1148. doi:10.1080/10473289.2003.10466268

Westhoff, M.C., H.H.G. Savenije, W.M.J. Luxemburg, G.S. Stelling, N.C. van de Giesen, J.S. Selker, L. Pfister, and S. Uhlenbrook. 2007. A distributed stream temperature model using high resolution temperature observations. Hydrol. Earth Syst. Sci. 11:1469–1480. doi:10.5194/hess-11-1469-2007